第 34 卷第 6 期
2018 年 6 月

无 机 化 学 学 报
CHINESE JOURNAL OF INORGANIC CHEMISTRY

Vol.34 No.6
1183-1191

电解液成分、厚度及表面改性对旋涂法制备的 $BiVO_4$ 膜层光电化学性能的影响

隋美蓉[1,2] 顾修全[3] 时梅林[2] 刘琳琳[2] 倪中海*,[1]

([1]中国矿业大学化工学院,徐州 221116)

([2]徐州医科大学医学影像学院,徐州 221004)

([3]中国矿业大学材料科学与工程学院,徐州 221116)

摘要:采用旋涂法在 FTO(SnO_2:F)导电玻璃衬底上沉积得到 $BiVO_4$ 多孔薄膜用以光解水,改变前驱体的浓度和旋涂次数以调控薄膜的厚度。研究了电解液成分、膜层厚度及表面改性等因素对刚经历过退火处理的 $BiVO_4$ 薄膜光电化学(PEC)性能的影响。结果表明:通过在电解液中添加适量的空穴吞噬剂 Na_2SO_3,或对表面进行 Co-Pi 改性均能有效改善 $BiVO_4$ 薄膜的 PEC 活性。这些措施均能有效抑制固液界面处的载流子复合反应。经 Co-Pi 改性的 $BiVO_4$ 薄膜在 0.6 V(vs SCE)偏压下,0.1 mol·L^{-1} Na_2SO_4+0.1 mol·L^{-1} Na_2SO_3 的电解液中展现出最高的光电流密度(4.3 mA·cm^{-2})。此外,选用一个代表性 $BiVO_4$ 薄膜作为光阳极制备了一个 PEC 生物传感器,在检测谷胱甘肽(GSH)上表现出比较高的灵敏度。本研究证实了 $BiVO_4$ 薄膜的 PEC 性能严重依赖着光俘获效率和载流子输运过程。

关键词:钒酸铋;光电化学;多孔膜;掺杂;修饰

中图分类号:TB34 **文献标识码**:A **文章编号**:1001-4861(2018)06-1183-09

DOI:10.11862/CJIC.2018.143

Effects of Electrolyte Composition, Thickness and Surface Modification on Photo-Electrochemical Activity of $BiVO_4$ Films Deposited through Spin-Coating

SUI Mei-Rong[1,2] GU Xiu-Quan[3] SHI Mei-Lin[2] LIU Lin-Lin[2] NI Zhong-Hai*,[1]

([1]*School of Chemical Engineering and Technology, China University of Mining and Technology, Xuzhou, Jiangsu* 221116, *China*)

([2]*College of Medical imaging, Xuzhou Medical University, Xuzhou, Jiangsu* 221004, *China*)

([3]*School of Materials Science and Engineering, China University of Mining and Technology, Xuzhou, Jiangsu* 221116, *China*)

Abstract: Porous $BiVO_4$ thin films have been prepared on the fluorine doped tin oxide (SnO_2:F) coated glass substrates through a facile spin-coating strategy for water splitting application. The film thickness was tuned by varying the deposition cycles and the precursor concentration, respectively. The influences of electrolyte composition, film thickness and surface modification were investigated on the actual photoelectrochemical (PEC) performance of the as-annealed $BiVO_4$ porous films. The results show that the PEC activity of $BiVO_4$ can be enhanced effectively by adding a hole scavenger Na_2SO_3 with suitable amount into the electrolyte, or modified the surface with a co-catalyst Co-Pi. These methods can suppress the carrier recombination that occurs at the solid/liquid interface. The highest photocurrent density (4.3 mA·cm^{-2} at a bias of 0.6 V (vs SCE)) was achieved in the $BiVO_4$ samples which were synthesized at the optimal condition and characterized under a visible-light irradiation intensity of 100 mW·cm^{-2}, using a 0.1 mol·L^{-1} Na_2SO_4+0.1 mol·L^{-1} Na_2SO_3 electrolyte. Additionally, a facile PEC bio-sensor is constructed by using a $BiVO_4$ film anode, leading to an acceptable sensitivity for detecting the

收稿日期:2018-01-18。收修改稿日期:2018-04-10。

中央高校基本科研业务费专项资金(No.2015XKZD08)资助项目。

*通信联系人。E-mail:nizhonghai@cumt.edu.cn;会员登记号:S06N0244M1703。

glutathione (GSH). In a word, it is demonstrated that the PEC performance of $BiVO_4$ is dependent on both the light harvesting and carrier diffusion process.

Keywords: $BiVO_4$; photoelectrochemical; porous films; doping; modification

0 Introduction

During the last few years, much attention has been paid to solar-driven water splitting, which is a low-cost technique for the utilization of solar energy to produce chemical fuels (such as H_2)[1-2]. There are three main ways for solar water splitting: photocatalysis, photoelectrochemical (PEC) cells, and the photovoltaic (PV) driven PEC cells[3]. Of them, the PEC method (*i.e.*, the PEC cell) owns the most ideal cost performance, thus it might be one of the most promising techniques for a large-scale application in near future. It is known that the photoanode is a key component of the PEC cell, which is always a semiconductor and can realize a conversion of solar energy to electricity.

As early as in 1967, Fujishima and Honda discovered that H_2 can be generated from a PEC cell which is consisted of a TiO_2 photoanode under an ultraviolet (UV) illumination[4]. Nevertheless, TiO_2 is a wide bandgap semiconductor (E_g=3.2~3.4 eV), which can only respond to UV light that accounts for 4% of incoming solar energy. Thus, it is necessary to either reduce the bandgap of TiO_2, modify with narrow-gap semiconductors or look for a new alternative photoanode[5-6]. Up to now, a number of semiconductor photoanodes have been developed to replace TiO_2 for operating under a visible light irradiation, including α-Fe_2O_3, WO_3, BiOBr, Ag_3PO_4, $BiVO_4$, $NiNb_2O_6$, and so on[7-12]. Of them, $BiVO_4$ represents one of the most promising photoanode candidates due to a plenty of advantages like non-toxicity, stability, low cost, narrow band gap of ~2.4 eV, as well as the suitable levels of the conduction band (CB) and valence band (VB)[13]. Fortunately, in a latest report, it has been demonstrated that a PEC device made of modified $BiVO_4$ and α-Fe_2O_3 as dual photoanodes shows an unbiased water splitting efficiency (or said, solar to hydrogen efficiency) of 7.7%[14]. Moreover, it is relatively easy to obtain a $BiVO_4$ porous thin film with controllable thickness due to the accessibility of a Bi-V-O precursor with good fluidity and dispersity [15]. Based on the above merits, similar with TiO_2, it has been demonstrated feasible to fabricate a $BiVO_4$ photoanode with both an inverse opal network structure and a considerable average pore size by using a dilute Bi-V-O precursor[16-17].

Theoretically, the maximum water oxidation photocurrent density (J_{max}) for $BiVO_4$ photoanodes under Air-mass 1.5 Global (AM 1.5G) solar illumination is 7.5 $mA\cdot cm^{-2}$[18]. Nevertheless, to the best of our knowledge, the reported photocurrent density (J) are much lower than the theoretical value (7.5 $mA\cdot cm^{-2}$), owing to a serous carrier recombination occurred at the electrolyte/electrolyte interface[19]. In other words, only a small part of photoexcited holes take part in the water oxidation reaction and make a contribution to the photocurrent output. So far, much effort has been devoted to improve the performance of $BiVO_4$ photoanodes, including the doping of hetero-ions (such as Mo^{6+}, W^{6+}, P^{5+}), surface modification and forma-tion of a heterostructure with other semiconductors[20-22], but few work is focused on the effect of layer thickness or electrolyte component on the PEC performance of $BiVO_4$. Surely, fewer attention is paid towards the mechanism why the performance of $BiVO_4$ porous thin film is improved.

In the present work, we will investigate the effect of preparation and characterization conditions on the PEC properties of porous $BiVO_4$ thin films which were synthesized on the fluorine doped tin oxide (FTO, also named as SnO_2:F) substrates through a facile spin-coating deposition method. After optimizing the preparation procedure, a photocurrent density of ~4.3 $mA\cdot cm^{-2}$ was achieved in the cobalt phosphate (Co-Pi) modified $BiVO_4$ layers under a visible-light

irradiation intensity of 100 mW·cm^{-2}. The mechanism for the performance improvement was analyzed by combining LSV plots with electrochemical impedance spectra (EIS).

1 Experimental

All the chemical reagents including bismuth nitrate pentahydrate ($Bi(NO_3)_3·5H_2O$, ≥98%), vanadyl acetylacetonate ($VO(acac)_2$, ≥98%), cobalt nitrate hexahydrate ($Co(NO_3)_2·6H_2O$, ≥98%), glacial acetic acid (CH_3CO_2H, ≥99.7%) and acetylacetone (≥99%) were analytically pure (AR) and purchased from Shanghai Civi Co., Ltd. Conductive FTO glass substrates (2.2 mm thick, 15 Ω·□$^{-1}$) were obtained from Yinkou OPV Tech Co., Ltd.

1.1 Preparation of porous $BiVO_4$ thin films

The actual concentration of precursor solution was determined by adding the Bi and V based salts (solute). For example, in order to prepare a 45 mmol·L^{-1} precursor solution for synthesizing $BiVO_4$ porous thin films, two different solutions were prepared by dissolving 0.131 g (0.27 mmol) of $Bi(NO_3)_3·5H_2O$ in 1 mL of acetic acid and 0.072 g (0.27 mmol) of $VO(acac)_2$ in 5 mL methanol. After pouring the solution containing Bi into that containing V slowly (or said, drop by drop), the mixture (n_{Bi}/n_V=1) was subjected to ultrasonicate robustly for 30 min, after which a stable, clear and straw-yellow precursor solution was obtained. This precursor was then employed in the following spin-coating procedure. Different concentrations (n_{Bi}/n_V=1) of precursor solution were obtained with the same methods.

The film deposition process involved a small amount (~125 μL) of precursor solution being spread over the whole FTO substrate (2 cm×2 cm) and the substrate was then spin-coated at 1 500 r·min for 20 s, as displayed in Fig.1. Afterwards, the film samples were transferred into an oven and dried at 150 ℃ for 5 min, followed by a further 400 ℃ annealing treatment for 2 h. The processes of spin-coating deposition and air-annealing were repeated several times to obtain a target thickness of the $BiVO_4$ porous thin film.

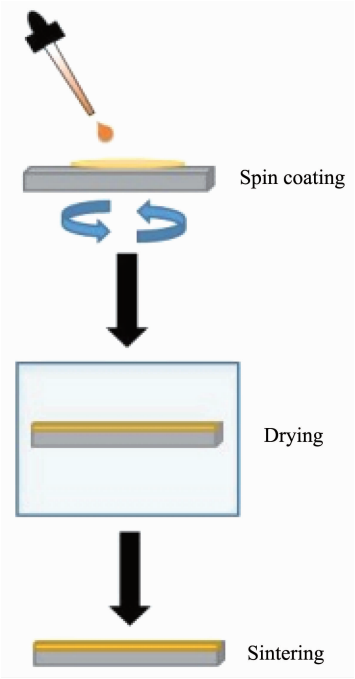

Fig.1 Schematic procedure for preparing $BiVO_4$ porous thin films

1.2 Photo-assisted Co-Pi electrodeposition

This technique was chosen for the deposition of Co-Pi because it provides a more efficient route of coupling Co-Pi to the $BiVO_4$ electrode than the common electrodeposition[20]. This technique involved a porous $BiVO_4$ thin film (working electrode, WE), an saturated calomel (reference electrode, RE) and a Pt foil (counter electrode, CE) being immersed in a 0.1 mol·L^{-1} sodium phosphate buffer (pH=7.0) containing 0.5 mmol·L^{-1} of Co^{2+} ions (from cobalt nitrate). A constant potential of 1.32 V versus saturated calomel electrode (SCE) was then applied for a certain period of time using an electrochemical workstation (CHI660D). In addition, the visible light (100 mW·cm^{-2}) from a 500 W Xe lamp was used to irradiate the $BiVO_4$ electrodes during the whole deposition process (lasting for 15 min).

1.3 Material characterization

The cross-sectional morphology and phase structure were characterized by a field emission scanning electron microscopy (FESEM, Sirion 200) operating at 5 kV and an X-ray diffraction (XRD, Haoyuan DX-2700) with a Cu $K\alpha$ source (λ=0.154 06 nm). X-ray tube voltage, current and scanning range

were set at 45 kV, 40 mA and 2θ=10°~80°, respectively. In addition, the diffuse absorption spectra of $BiVO_4$ porous thin films were measured on a Cary 300 UV-Vis spectrophotometer with integrating sphere (Varian, USA). The composition of a Co-Pi modified $BiVO_4$ film was characterized by an electron probe micro-analyzer (EPMA-8050G, Shimadzu, Japan).

1.4 PEC measurements

The PEC performance was measured by an electrochemical workstation (CHI660D) under irradiation. The visible-light irradiation was provided by a 500 W Xe lamp (Beijing Trusttech Technology Co., Ltd.) with using a UV cut-off filter. The $BiVO_4$ porous thin films were employed as the working electrode (WE), and they were coated with a non-conductive epoxy, leaving an active area of 1 cm×1 cm. Additionally, a Pt foil and a SCE were used as the counter electrode (CE) and reference electrode (RE), respectively. The electrolyte is a mixed aqueous solution of Na_2SO_4 and Na_2SO_3.

Linear sweep voltammogram (LSV) plots were gained under visible light irradiation, while the Mott-Schotty plots were measured in dark at a constant frequency of 1 kHz. The Nyquist plots were obtained at a potential of 0 V (vs SCE) by a choice of alternating current impedance technology at a frequency range from 10^{-2} to 10^5 Hz. For all the PEC measurements, a front-side illumination of the $BiVO_4$ working electrodes was employed. On the basis of this, the fabricated $BiVO_4$ electrode was further adopted as a PEC bio-sensing platform (also said, the bio-sensor) for detecting the glutathione (GSH). The bioanalysis of the GSH concentration was examined by performing the transient photocurrent (*J-t*) plots at a bias of 0 V (vs SCE) and under irradiation.

2 Results and discussion

Fig.2 shows the typical XRD pattern, cross-sectional SEM image and UV-Vis spectrum. It is clearly seen that the $BiVO_4$ film exhibits a monoclinic structure, since that all the peaks can be assigned to PDF No.14-688 and except those from a FTO layer (Fig.2a). It is also found that the $BiVO_4$ porous thin film displays a good visible light response, while the film thickness is around 120 nm (Fig.2b). An abrupt absorption edge appears around 500 nm, which is consistent with the bandgap of $BiVO_4$ (~2.4 eV).

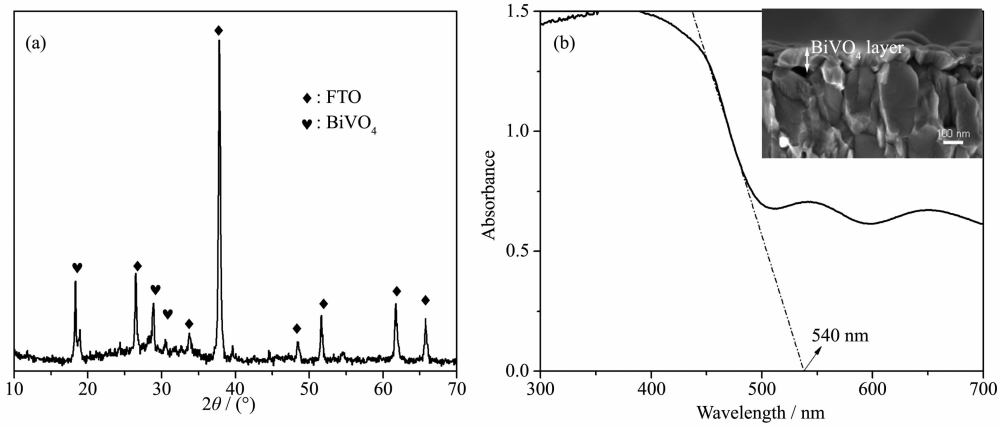

Inset displays a typical cross-sectional FESEM image of a $BiVO_4$ thin film prepared in precursor concentration of 45 mmol·L^{-1} with 5 layers

Fig.2 Typical XRD pattern (a) and optical absorption spectra (b) of $BiVO_4$ porous thin films which were deposited on FTO substrates (5 cycles) directly

2.1 Effect of electrolyte composition

Fig.3 shows the influence of electrolyte component on the actual PEC performance of the $BiVO_4$ films. It is found that the photocurrent density is independent on the electrolyte concentration while strongly dependent on the electrolyte composition. In details, no obvious changes are observed in the LSV or *J-t* plots with only increasing the concentration of Na_2SO_4 from 0.1 to 1.0 mol·L^{-1}, while the photocurrent is enhanced significantly after adding 0.1

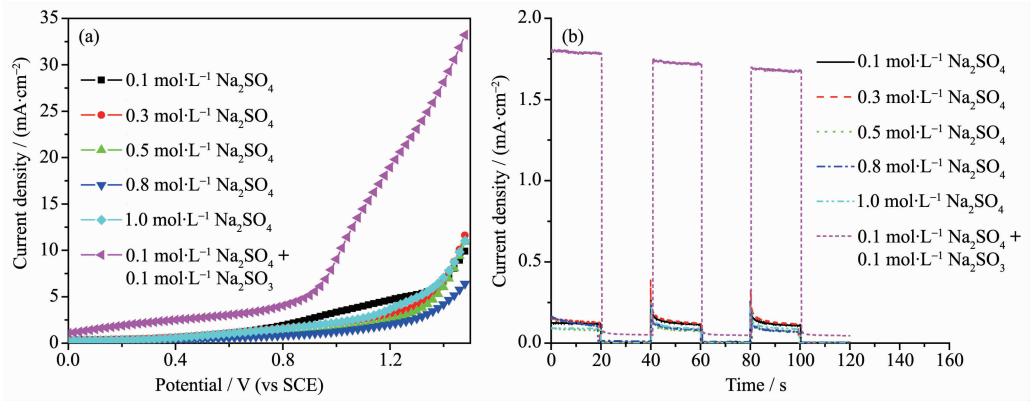

Plots in (b) are measured at a bias of 0.6 V (vs SCE)

Fig.3　LSV plots (a) and *J-t* plots under a chopped irradiation (b) of $BiVO_4$ thin porous films laid in different electrolytes containing of Na_2SO_3 and Na_2SO_4

mol·L^{-1} Na_2SO_3 into the 0.1 mol·L^{-1} Na_2SO_4 solution. It suggests that the performance of a photoanode is very sensitive to the hole scavenger Na_2SO_3 in the electrolyte. Namely, the anion SO_3^{2-} could react with the photoexcited holes more easily than OH^- in the water, leading to a large enhancement of the photocurrent density.

2.2　Effect of precursor concentrations

Fig.4 displays the cross-sectional SEM images of $BiVO_4$ synthesized by using the precursors with various concentrations. Apparently, the thicker the precursor solution, the larger thickness is the $BiVO_4$ layer. It is reasonable that the films are thickened from ~30 to ~210 nm with increasing the precursor concentration from 15 to 60 mmol·L^{-1}, while they display a porous structure due to the evaporation of organic components. Of these samples, the one deposited at a precursor concentration of 45 mmol·L^{-1} displays a film thickness of ~120 nm.

Fig.5 displays the UV-Vis absorption spectra of the $BiVO_4$ films with different precursor concentrations. Apparently, the visible-light harvesting of the photoanode gets enhanced a lot with increasing the precursor concentration, which is a result of the improved film thickness. Besides, it is also found that the optical bandgap (E_g) is reduced slightly due to a larger influence of the $BiVO_4$ in the entire $BiVO_4$/FTO

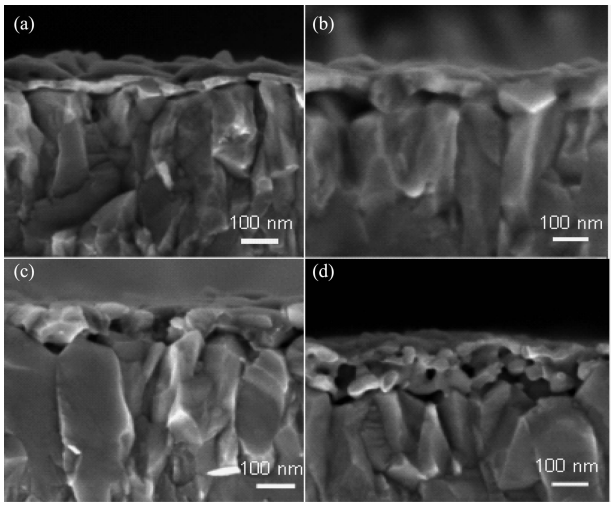

Fig.4　Cross-sectional FESEM images of $BiVO_4$ porous thin films fabricated in different precursor concentrations of (a) 15, (b) 30, (c) 45 and (d) 60 mmol·L^{-1} with a constant cycle number of 5

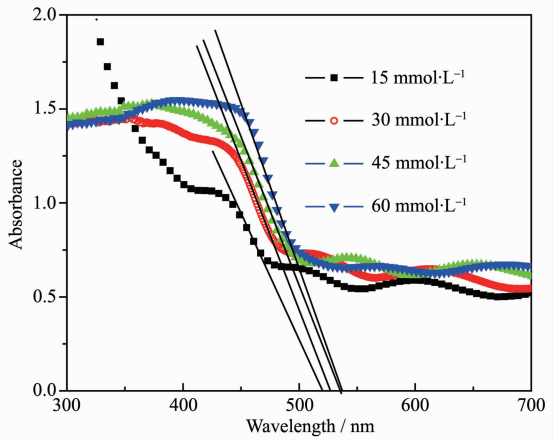

Fig.5　UV-Vis diffusion absorption spectra of $BiVO_4$ porous thin films fabricated in different concentrations of the precursor solution (from 15 to 60 mmol·L^{-1}) using a constant cycle number of 5

bilayered films. It is known that $BiVO_4$ owns a narrower bandgap (E_g=2.4 eV) than FTO (E_g=3.6~4.0 eV), thus a larger content ratio of $BiVO_4$/FTO would result in a narrower bandgap of the sample.

Fig.6 also displays the LSV plots of $BiVO_4$ films with different concentrations of precursor. It is observed that the highest photocurrent density (1.49 $mA\cdot cm^{-2}$ at 0.6 V (vs SCE)) appears in the $BiVO_4$ film deposited using a 45 $mmol\cdot L^{-1}$ precursor solution. It is easily understood that an increase of film thickness facilitates enhancing the light harvesting of a photoanode. However, the actual photocurrent is also limited by the poor carrier diffusion lengths of $BiVO_4$ polycrystalline films, which results in a decrease of the photocurrent as the precursor concentration increases from 45 to 60 $mmol\cdot L^{-1}$.

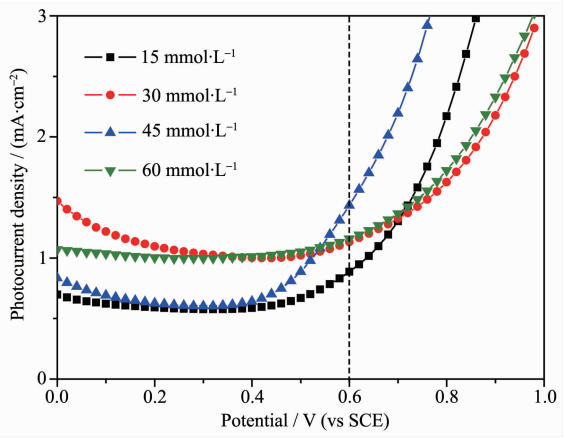

Electrolyte: 0.1 $mol\cdot L^{-1}$ Na_2SO_4+0.1 $mol\cdot L^{-1}$ Na_2SO_3 solution; active area: 1 cm^2

Fig.6 LSV plots under a continuous irradiation of $BiVO_4$ porous thin films which were prepared using different concentrations of precursor solution

2.3 Effect of deposition cycles

Fig.7 indicates the cross-sectional SEM images of $BiVO_4$ films deposited with various layer numbers. As expected, both the thickness and porosity are enhanced significantly after increasing the layer number from 2 to 10. Apparently, it can reach the identical effect with an increase of precursor concentration. Accordingly, the effect of deposition cycles (namely, layer numbers) on the PEC activity is also examined in Fig.8. It is clearly observed that the $BiVO_4$ sample with 5 deposition cycles displays the highest photocurrent value at 0.6 V (vs SCE) of all. In other words, when the layer number exceeds 5, the photocurrent is reduced accordingly due to a limitation of the charge carrier diffusion length. That is to say, the optimal PEC performance is achieved in the $BiVO_4$ films with a layer number of 5 or thickness of ~120 nm.

Further, we also assembled a PEC sensor by using a porous $BiVO_4$ film electrode, and the bio-

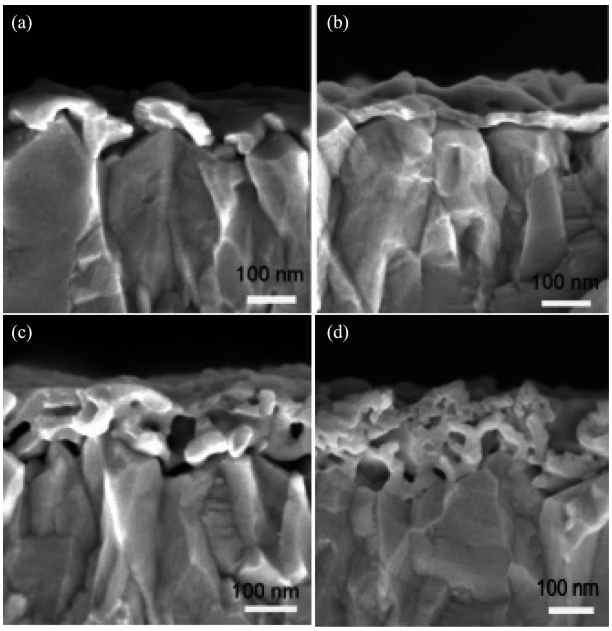

Fig.7 Cross-sectional FESEM images of $BiVO_4$ porous thin films fabricated using a precursor concentration of 45 $mmol\cdot L^{-1}$ and different layer number of (a) 2, (b) 5, (c) 7 and (d) 10

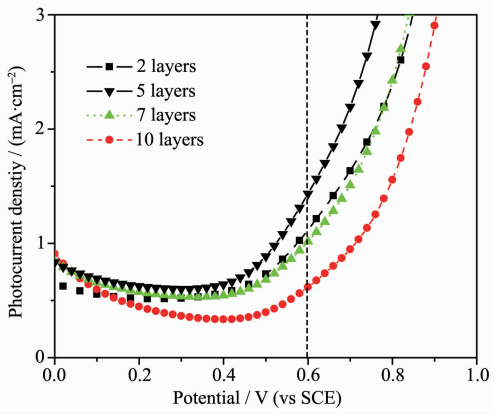

Precursor concentration: 45 $mmmol\cdot L^{-1}$; electrolyte: 0.1 $mol\cdot L^{-1}$ Na_2SO_4+0.1 $mol\cdot L^{-1}$ Na_2SO_3 solution; active area: ~1 cm^2

Fig.8 LSV plots under a continuous irradiation of $BiVO_4$ porous thin films prepared using different layer numbers

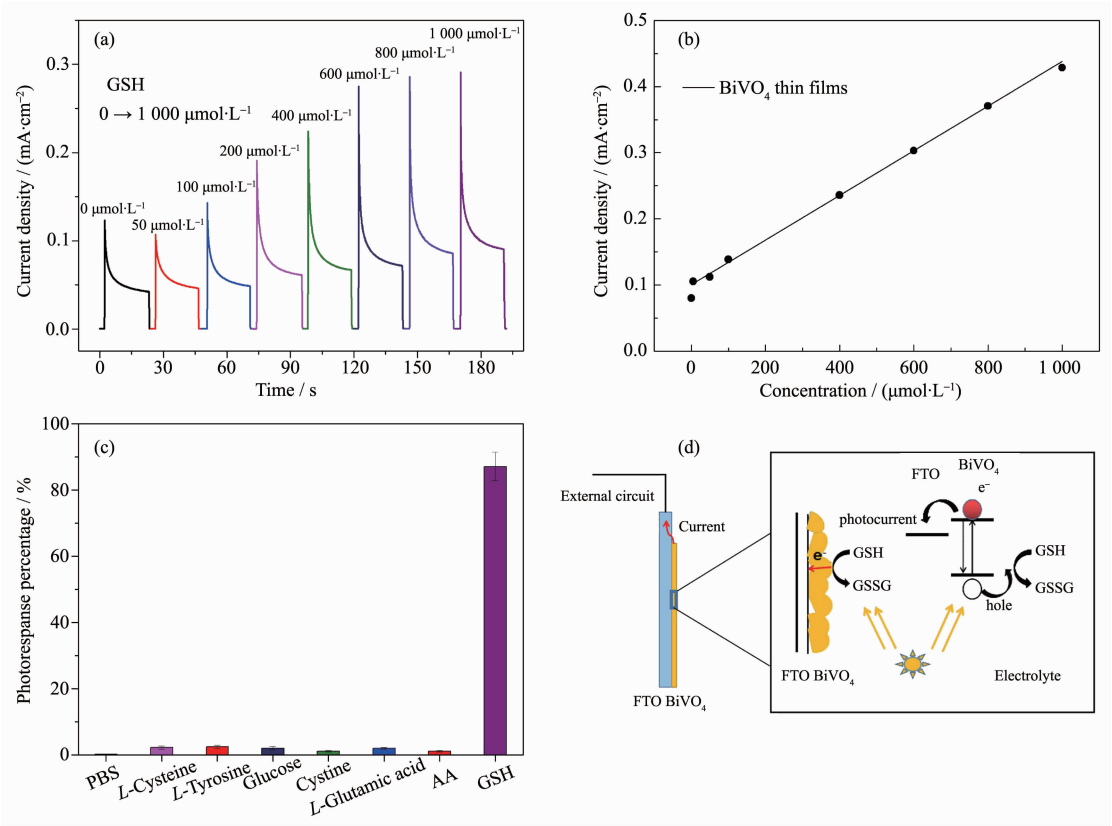

Fig.9　Amperometric *J-t* plots (a) and linear relationship between photocurrent density and GSH concentration (b) of a $BiVO_4$ PEC bio-sensor with an addition of GSH to reach the concentrations of 0~1 000 μmmol·L^{-1} in the electrolyte; (c) Selectivity experiment by testing in the solutions containing different organic interferents including PBS, *L*-Cystenine, *L*-Tyrosine, Glucose, Cystine, *L*-Glutamic Acid, AA, where the concentrations of these interferents are 20 μmol·L^{-1} while that of GSH is 100 μmol·L^{-1}; (d) Possible mechanism for the PEC detection of GSH

sensing performance of this device was measured at zero bias (0 V vs SCE), as indicated in Fig.9. Herein, the $BiVO_4$ film was fabricated under the optimal condition (45 mmol·L^{-1} and 5 layers). At first, a series of sharp peaks in the *J-t* plots (similar with the phenomenon appeared in references[23-24]), suggesting that there is an instability in the photocurrent (Fig.9a). Such a behavior may be due to the poor charge separation on $BiVO_4$ surfaces or interfaces under zero bias. Besides, with increasing the GSH concentration (from 0 to 1 000 μmol·L^{-1}), the photo-response is enhanced significantly, which displays an acceptable sensitivity for detecting the GSH (Fig.9b). And also, this $BiVO_4$ biosensor also exhibits much higher photo-response towards detection of GSH than other additives (Fig.9c), which was attributed to the higher redox capability of GSH. Namely, it was easy to realize a conversion of GSH to the oxidized glutathione (GSSG) through the following reaction[25]: $2GSH+2h^{+}+2OH^{-}\rightarrow GSSG+2H_2O$. The possible mechanism for the PEC detection of GSH is shown in Fig.9d. Apparently, under a visible light irradiation, a number of electron-hole pairs are produced inside a porous $BiVO_4$ film. The existence of the GSH species in an electrolyte accelerates the consumption of holes, leading to a faster migration of the electron towards the opposite direction (*i.e.*, the photocurrent). In other words, the GSH plays a role of the hole sacrificial agent, leading to an acceleration of the carrier separation and an enhancement of the photocurrent output.

2.4　Effect of Co-Pi modification

In this section, the effect a Co-Pi modification was investigated on the PEC activity of a $BiVO_4$ electrode. Table 1 displays the actual composition of the Co-Pi/$BiVO_4$ film sample. The elements of Co and

P are clearly identified with considerable contents, which demonstrates a success in the Co-Pi modification. Note that all the elements (Bi, V, Co, *etc*.) could be viewed as the oxides exist in the sample, where the elements Na, Si and Ca are from the glass substrate.

Table 1 Composition analysis of the Co-Pi modified $BiVO_4$ thin film via an electron microprobe

Oxide	Mass fraction / %	Atom fraction / %
Na_2O	3.57	12.76
SiO_2	2.19	6.41
P_2O_5	5.33	14.14
SO_3	0.42	1.07
C1	0.21	0.49
CaO	0.93	1.90
V_2O_5	3.50	5.65
CoO	11.18	15.59
SnO_2	44.93	31.1
Bi_2O_5	27.74	10.09
Total	100.00	100.00

Fig.10 displays a comparison of the LSV plots of $BiVO_4$ films before and after Co-Pi modification. Apparently, the photocurrent of a $BiVO_4$ electrode is enhanced a lot after coating with a co-catalyst Co-Pi, reaching to a value of 4.3 mA·cm^{-2} at a bias of 0.6 V (vs SCE). Such a value is comparable to several previous reports. Further, the mechanism for the performance enhancement is also revealed through an EIS analysis, including the Nyquist and Mott-Schotty plots displayed in Fig.11a and 11b, respectively. Typically, during an equivalent circuit model displayed in the inset of Fig. 11a, R_S represents the series resistance from the solid electrode, electrolyte and wires, while R_{CT} represents the charge transfer resistance occurred at the electrode/electrolyte interface. As indicated in Table 2, the parameters N_d and V_{fb} represent the donor concentration and flat-band potential of a $BiVO_4$ film electrode, respectively. Both of them can be determined from a linear fitting of the Mott-Schotty plots in Fig.11b. Herein, N_d is inversely proportional to the slope of the fitted curve, while V_{fb} corresponds to the intercept of the fitted plot on the X-axis. Notably, after a Co-Pi modification, R_{CT} gets smaller while V_{fb} becomes more positive, implying that the charge transfer resistance is reduced a lot. That is to say, the PEC performance enhancement is attributed to a more efficient interfacial charge transfer process.

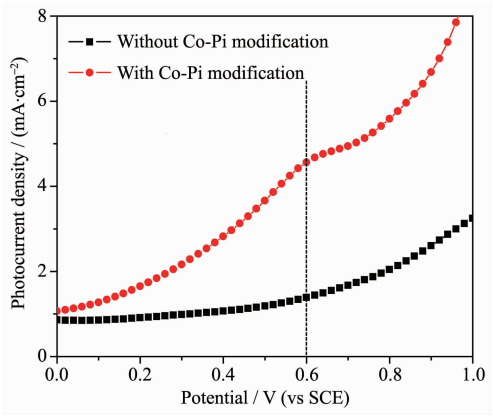

Precursor concentration: 45 mmmol·L^{-1}; Layer: 5; Electrolyte: 0.1 mol·L^{-1} Na_2SO_4+0.1 mol·L^{-1} Na_2SO_3 solution

Fig.10 LSV plots under a continuous irradiation of $BiVO_4$ porous thin films with and without the Co-Pi modification

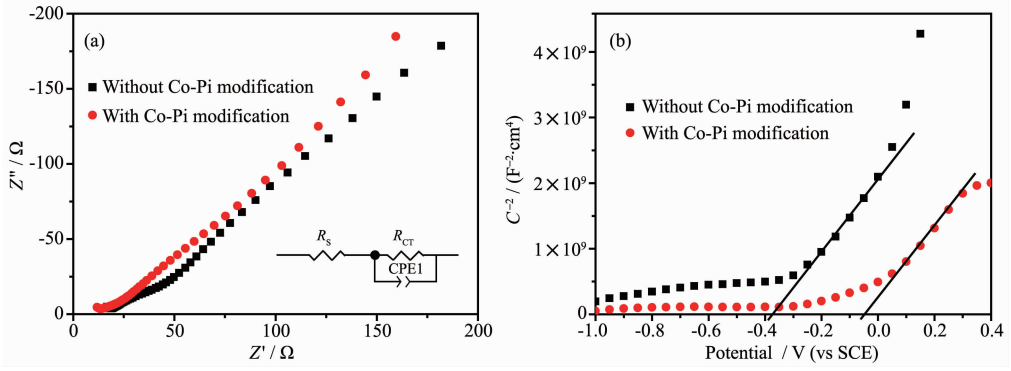

Inset of (a) is an equivalent circuit model for fitting the plots

Fig.11 Comparison on the Nyquist (a) and Mott-Schotty plots (b) of $BiVO_4$ porous thin films with and without the Co-Pi modification

Table 2　Calculated electronic parameters from Nyquist plots under illumination and Mott-Schotty plots measured in dark of $BiVO_4$ electrodes by terms of the corresponding model or formula[24]

Sample	R_S / Ω	R_{CT} / Ω	N_d / cm^{-3}	V_{fb} / V (vs SCE)
without the Co-Pi modification	18.38	6.47×10^{10}	1.0×10^{18}	−0.38
with the Co-Pi modification	14.68	4.77×10^{10}	1.0×10^{18}	−0.05

3　Conclusions

$BiVO_4$ porous thin films have been prepared through a facile spin-coating route, followed by an air-annealing treatment process for PEC applications. The effects of electrolyte composition and preparation parameters (layer thickness) were investigated, too. The PEC activity of $BiVO_4$ could be enhanced efficiently by adding the hole scavenger SO_3^{2-} into the electrolyte. Otherwise, it was also found that the $BiVO_4$ film exhibit the optimal PEC performance (~4.3 $mA\cdot cm^{-2}$) after using a 45 $mmol\cdot L^{-1}$ precursor, depositing for 5 layers (with a thickness of ~120 nm) and modifying with Co-Pi thin layer, and using a 0.1 $mol\cdot L^{-1}$ Na_2SO_4+0.1 $mol\cdot L^{-1}$ Na_2SO_3 solution as the electrolyte. Finally, a PEC bio-sensor based on $BiVO_4$ has been fabricated for detecting the GSH, leading to an acceptable sensitivity.

References:

[1] Chen X B, Li C, Grtzel M, et al. *Chem. Soc. Rev.*, **2012**,**41**: 7909-7937

[2] Ma Y, Wang X L, Jia Y S, et al. *Chem. Soc. Rev.*, **2014**,**114** (19):9987-10043

[3] Zhang X F, Zhang B Y, Cao K, et al. *J. Mater. Chem. A*, **2015**, **3**:21630-21636

[4] Fujishima H, Honda K. *Nature*, **1972**,**238**:37-38

[5] YUAN Su-Jun(袁素珺), ZHANG Qing-Hong(张青红), LEI Fang(雷芳), et al. *Chinese J. Inorg. Chem.*(无机化学学报), **2015**,**31**(6):1099-1104

[6] XU Zhen(许贞), LI Juan(李娟), LI Xin-Jun(李新军). *Chinese J. Inorg. Chem.*(无机化学学报), **2013**,**29**(3):429-436

[7] Mayer M T, Lin Y, Yuan G, et al. *Acc. Chem. Res.*, **2013**,**46** (7):1558-1566

[8] Hong S J, Lee S, Jang J S, et al. *Energy Environ. Sci.*, **2011**, **4**:1781-1787

[9] Li K, Zhang H B, Tang Y P, et al. *Appl. Catal. B*, **2015**,**164**: 82-91

[10]Sui M R, Han C P, Wang Y, et al. *J. Mater. Sci.-Mater. Electron.*, **2016**,**27**:4290-4296

[11]Zhang S, Gu X Q, Zhao Y L, et al. *Mater. Sci. Eng. B*, **2015**,**201**:57-65

[12]ZHANG Yan(张妍), YU Jian-Qiang(于建强), GAO Xing-Long(高行龙), et al. *Chinese J. Inorg. Chem.*(无机化学学报), **2011**,**27**(1):141-144

[13]Li J T, Wu N Q. *Catal. Sci. Technol.*, **2015**,**5**:1360-1384

[14]Kim J H, Jang J W, Jo Y H, et al. *Nat. Commun.*, **2016**,**7**: 13380 (9 Pages)

[15]Sayama K, Nomura A, Zou Z, et al. *Chem. Commun.*, **2003** (23):2908-2909

[16]Ma M, Kim J K, Zhang K, et al. *Chem. Mater.*, **2014**,**26**: 5592-5597

[17]Zhang L W, Reisner E, Baumberg J J. *Energy Environ. Sci.*, **2014**,**7**:1402-1408

[18]Park Y, McDonald K J, Choi K S. *Chem. Soc. Rev.*, **2013**, **42**:2321-2337

[19]Zhong D K, Choi S, Gamelin D R. *J. Am. Chem. Soc.*, **2011**, **133**:18370-18377

[20]Thalluri S M, Hernández S, Bensaid S, et al. *Appl. Catal., B*, **2016**,**180**:630-636

[21]Jo W J, Jang J W, Kong K, et al. *Angew. Chem. Int. Ed.*, **2012**,***51***(13):3147-3151

[22]Rao P M, Cai L L, Liu C, et al. *Nano Lett.*, **2014**,**14**(2):1099 -1105

[23]Ng Y H, Iwase A, Kudo A, et al. *J. Phys. Chem. Lett.*, **2010**,**1** (17):2607-2612

[24]Zhang S, Gu X Q, Zhao Y L, et al. *J. Electron. Mater.*, **2016**, **45**(1):648-653

[25]Zhao K, Yan X Q, Gu Y S, et al. *Small*, **2016**,**12**(2):245-251